

SYNTHESIS AND CHARACTERIZATION OF ZINC AND MANGANESE-DOPED ENSTATITE AND ZINC-DOPED TALC

MANUELA CATALANO

Dipartimento di Fisica, Università della Calabria, Via P. Bucci, 87036 Arcavacata di Rende (CS)

INTRODUCTION

Since decades, particular interest has been addressed by researchers in the synthesis and study of silicates such as enstatite MgSiO_3 and talc $\text{Mg}_3\text{Si}_4\text{O}_{10}(\text{OH})_2$. Enstatite is useful for several technological applications such as substrates in electronics, high frequency insulators, thermal insulators in high temperatures applications, as luminescent materials in laser technology and more recently as suitable dielectric materials for millimeter wave communication (Höland & Beall, 2002; Ohsato, 2004; Song *et al.*, 2008; Sun & Kim, 2012). Talc, because of the low cost and good properties (*i.e.*, resistance to heat and acids, hydrophoby, electrical insulation), is widely used in many different products such as ceramics, papers, cosmetics, foods, polymers and filler in composites. The usual presence of foreign ions (*e.g.*, Mn, Ti, Ni) and their inconstant amounts in natural enstatite and talc hinder the use of these minerals as high-performance materials. For these reasons, enstatite doped with various elements such as Eu^{2+} , Dy^{3+} , Cr^{3+} , Li^+ , Sc^{3+} , Ni^{2+} , and Ti^{4+} (Moncorgè *et al.*, 1999; Smyth & Ito, 1977; Lin *et al.*, 2006; Bloise *et al.*, 2011) and talc doped with Ni, Co, Fe, S, O, Mg, $\text{Mg}(\text{NO}_3)_2$, and Mn (Wilkins & Ito, 1967; Ishida, 1990; Kirak *et al.*, 1999; Bloise *et al.*, 2010; Pidluzhna *et al.*, 2012) have been grown and characterized in several different ways. Nevertheless, there are still various problems to be solved in order to obtain very high quality crystals and the desired changes in their physical and chemical properties when they are doped with foreign elements.

The aims of this work are:

1) the growth of enstatite by slow cooling flux method in order to obtain large single crystals and to study how some of their chemical and physical characteristics change by varying the amount of zinc and manganese content. The slow cooling flux method was preferred to other methods (*e.g.*, sol-gel) because of the possibility to obtain large single crystals useful for the evaluation of the quality of the crystals obtained (*e.g.*, crystallinity, uniformity, purity);

2) the synthesis and characterization of several members of Zn-doped talc, starting with the Zn free talc end-member and moving on to talc grown in the presence of increasing amounts of Zn in order to assess unambiguously its influence on the chemical/physical properties (*e.g.*, morphology, thermal stability) by excluding the influence of other ions (*e.g.*, Fe, Ni, Al) commonly present in natural samples.

SYNTHESES

Synthesis of Zn and Mn-doped enstatite

Zn- and Mn-doped enstatite was produced by slow-cooling flux growth method, using MoO_3 , V_2O_5 , and Li_2CO_3 as melting agent and granular quartz, magnesium oxide, zinc oxide, and manganese oxide as nutrients. To increase the reactivity between nutrients, starting oxides were preheated in a vertical furnace. Several starting mixtures, with different MnO or ZnO concentrations, were first held at 1350 °C, 1250 °C, 1050 °C, and 950 °C and then slowly cooled down to 750-600 °C with different cooling rate (3.75 °C/h, 2.1 °C/h, 1.8 °C/h, 1.7 °C/h, Table 1). Un-doped enstatite was also synthesized for comparison.

Synthesis of Zn-doped talc

Talc was obtained under hydrothermal conditions. In order to grow Zn-doped talc, the following starting materials were used: granular quartz, magnesium oxide, and zinc oxide according to the stoichiometry of talc.

Table 1 - Molar ratios of the starting nutrient mixtures, experimental conditions and products obtained. Mg-En = enstatite; Mn-En = Mn-doped enstatite; Qtz = quartz; Br = braunite; Zn-En = Zn-doped enstatite; L-W = $\text{Li}_2\text{ZnSiO}_4\text{-Zn}_2\text{SiO}_4$ solid solution.

| Run | Nutrient (molar ratio) | | | | Cooling rate (°C/h) | Minerals produced | Average dopant in enstatite (wt.%) |
|-----|------------------------|------------------|------|------|---------------------|-------------------|------------------------------------|
| | MgO | SiO ₂ | MnO | ZnO | | | |
| H1 | 1.00 | 1.00 | - | - | 3.7 | Mg-En > Qtz | - |
| EN1 | 0.50 | 1.00 | 0.50 | - | 3.7 | Mn-En > Qtz | 8.87 |
| EN2 | 0.75 | 1.00 | 0.25 | - | 3.7 | Mn-En > Qtz, | 6.35 |
| EN3 | 0.60 | 1.00 | 0.40 | - | 2.1 | Mn-En > Qtz | 6.30 |
| EN4 | 0.25 | 1.00 | 0.75 | - | 2.1 | Br > Qtz | - |
| EN5 | 0.00 | 1.00 | 1.00 | - | 2.1 | Qtz > Br | - |
| EN6 | 0.50 | 1.00 | 0.50 | - | 1.7 | Mn-En > Qtz | 8.56 |
| EN7 | 0.60 | 1.00 | 0.40 | - | 1.7 | Mn-En > Qtz | 6.28 |
| EN8 | 0.40 | 1.00 | 0.60 | - | 1.7 | Mn-En > Qtz | 9.89 |
| EN9 | 0.00 | 1.00 | 1.00 | - | 1.7 | Br > Qtz | - |
| A2 | 0.80 | 1.00 | - | 0.20 | 2.1 | Zn-En, L-W | 3.57 |
| A1 | 0.60 | 1.00 | - | 0.40 | 2.1 | Zn-En, Qtz, L-W | 3.37 |
| A3 | 0.50 | 1.00 | - | 0.50 | 2.1 | Zn-En, L-W, Qtz | 3.48 |
| B2 | 0.40 | 1.00 | - | 0.60 | 1.7 | Zn-En | 10.49 |
| B1 | 0.20 | 1.00 | - | 0.80 | 1.7 | Qtz, L-W | - |
| C1 | 0.80 | 1.00 | - | 0.20 | 1.8 | Qtz, L-W, Zn-En | 4.53 |
| C2 | 0.50 | 1.00 | - | 0.50 | 1.8 | Qtz, Zn-En, L-W | 4.45 |
| I1 | 0.75 | 1.00 | - | 0.25 | 3.7 | Zn-En, Qtz | 4.43 |
| I3 | 0.25 | 1.00 | - | 0.75 | 3.7 | Qtz, L-W | - |

To increase the reactivity between nutrients, starting oxides were preheated in a vertical furnace. About 80 mg of finely powdered starting mixture, milled in an agate mortar (< 0.177 mm), was mixed with three different types of reactant in amount of 4 wt.% or 12 wt.%. *i*) H₂O; *ii*) H₂O + CaCl₂ (pH = 7); *iii*) H₂O + HCl (pH = 5), (see Table 2). Each mixture was sealed in a platinum capsule with an arc-welder and put to react in externally heated pressure vessel. Several runs were carried out at three different temperatures (300 °C, 500, and 650 °C) pressure of 2 kbar and reaction time of 160 hours (Catalano *et al.*, 2014). The capsules were finally rapidly quenched in water. Un-doped talc was also synthesized to be compared with the doped one.

Table 2 - Experimental conditions (P = 2 kbar, reaction time 160 h) and products obtained for each synthesis in order of decreasing abundance as detected by XRPD and SEM. α = H₂O 12%; β = H₂O + CaCl₂ 12%; γ = H₂O + HCl 12%; τ = H₂O 4%; Tlc = talc, W = willemite, Qtz = quartz, S = silicon dioxide, C = cristobalite, Z = zinc oxide, Zc = zincite.

| Run | Molar ratio | | T (°C) | Reactant | Detected phases | ZnO dopant average (wt.%) |
|-------|-------------|-----|--------|----------|-----------------|---------------------------|
| | MgO | ZnO | | | | |
| T1P | 3 | 0 | 650 | α | Tlc | 0.00 |
| T2e | 2 | 1 | 650 | α | Tlc, Qtz, W | 7.56 |
| T3f | 1.5 | 1.5 | 650 | α | Tlc, Qtz, W | 7.72 |
| T4 | 0 | 3 | 650 | α | W, Qtz, Zc | 0.00 |
| T2Ca | 2 | 1 | 650 | β | Z, S, C, Tlc | 9.06 |
| T3Ca | 1.5 | 1.5 | 650 | β | Z, S, C, Tlc | 7.53 |
| T2HCl | 2 | 1 | 650 | γ | Tlc, W, Qtz | 8.63 |
| T4HCl | 0 | 3 | 650 | γ | W, Qtz | 0.00 |
| T2a | 2 | 1 | 500 | τ | Tlc, Qtz, W | 10.68 |
| T2b | 2 | 1 | 500 | α | Tlc, Qtz, W | 6.92 |
| T2c | 2 | 1 | 300 | τ | C, Tlc, W | 15.16 |
| T2d | 2 | 1 | 300 | α | Qtz, Tlc, W | 16.40 |

EXPERIMENTAL METHODS

The starting materials and the final products obtained were characterized and studied by binocular microscope, X-ray powder diffraction (XRPD), scanning electron microscopy with energy dispersive spectrometry (SEM/EDS), single-crystal X-ray diffraction (XRD), micro-Raman (μ R), cathodoluminescence (CL), differential scanning calorimetry, thermogravimetric analysis (DSC-TG) and Fourier transform infrared spectroscopy (FT-IR).

CHARACTERIZATION

Zn and Mn-doped enstatite characterization

Zn- and Mn doped enstatite crystals were colorless and reddish/pale pink, respectively and they all appeared to be idiomorphic, commonly without defects and elongated along the *c*-axis (Fig. 1a, b).

Inspections of the recovered Zn and Mn-doped enstatite crystals revealed that they were virtually free of fluid inclusions. In some rare specimens, veins occurred, which were open towards both ends and contained some quench material. According to the XRPD patterns, the most intense diffraction peaks of Zn and Mn-doped enstatite consisted of orthoenstatite (OR-EN; JCPDS 22-0714) associated with clinoenstatite (CL-EN; JCPDS 35-610).

The formation of clinoenstatite by quenching at 600 °C and higher temperatures was probably due to shearing orthoenstatite (Turner *et al.*, 1960). Fast cooling cannot be invoked as a consequence of the growth of clinoenstatite (Ushio *et al.*, 1991), because it was found also in the run with slower cooling rate (*i.e.*, 1.7 °C/h).

When the content of ZnO was increased in the starting mixtures, the decrease of flux acidity gave the formation of other phases such as VO₂, Li₂MoO₄ and Li₂Si₂O₅, (XRPD detected). When enstatite was doped with manganese, the formation of side products from the flux was avoided.

As concern morphology, more often Zn-doped enstatite crystals grew as intergrowths of single crystals parallel to the *c*-axis (Fig. 1c) with the maximum length of 3.5 mm.

Conversely, Mn-doped enstatite grew as single prismatic crystals of different size (Fig. 1d), with well-developed (100), (011), (010), (110), (0 $\bar{1}1$), ($\bar{1}\bar{1}0$) and ($\bar{1}\bar{1}0$) faces and reached the dimensions of more than 8 mm in length.

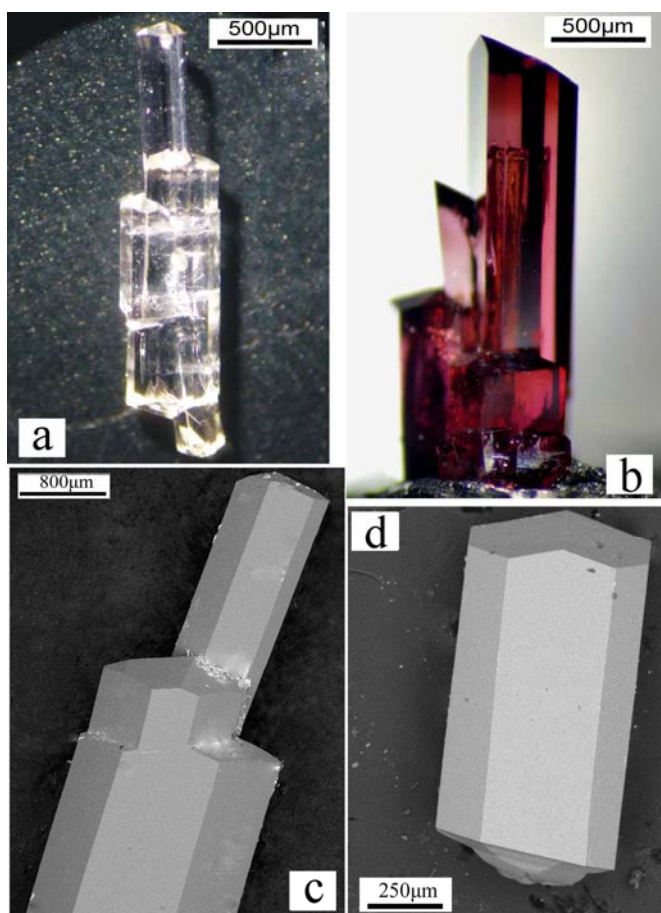


Fig. 1 - a) Optical image of transparent crystals of Zn-doped enstatite; b) optical image of reddish crystals of Mn-doped enstatite; c) secondary electron SEM images of Zn-doped enstatite intergrowth crystals; d) secondary electron SEM images of Mn-doped enstatite single crystal.

Even if normally crystals grown under slow cooling rate, they were more than one order of magnitude bigger (by volume) than those crystallized during faster cooling; the size of both Zn and Mn-doped enstatite seems not to be related to the cooling rate. However, when enstatite was doped with manganese, an inverse correlation between size and amount of MnO dopant (wt.%) was observed; crystals size estimated by SEM images showed a decreasing tendency with the increase in Mn concentration (see EN2 and EN8 in Table 1). Probably, Mn acted as inhibitor of the growth: high amount of Mn atoms could hinder the diffusion of the nutrients, thus decreasing the growth rate of the crystals during the reaction and resulting in crystals smaller in size (Sangwal, 1996).

In regard to the chemical composition, quantitative analyses (SEM/EDS), carried out on 10 single crystals for each run, showed that the amount of Zn^{2+} and Mn^{2+} indicated as MnO and ZnO wt.% ranges from 6.28 wt.% to 9.89 wt.% and from 3.37 to 10.49 wt.%, respectively. A direct correlation was observed between Mn concentration in the starting mixture and Mn-dopant in the grown enstatite crystals even if the increase was not proportional to the amount of Mn present in the starting mixture. The behaviour of zinc was more complicated; indeed, Zn-doped enstatite crystals shifted from their stoichiometric composition in the ideal products of the starting mixtures. Probably, this was due to the growth of phases that subtract zinc from the starting materials such as Li_2ZnSiO_4 - Zn_2SiO_4 (see Table 1). Moreover, it was probable that the starting temperature played a key role in the case of the presence of zinc as dopant in terms of its solubility. In fact, the lower starting temperature could cause a minor solubility of zinc in the melt with a consequent formation of enstatite with lower amount of Zn in its lattice.

No enstatite was obtained when Zn or Mn were totally in substitution for Mg in the starting mixtures. Probably the different characteristic of Zn^{2+} and Mn^{2+} respect to Mg^{2+} might result in the deformation of the crystal structure; therefore, it was not possible to obtain $ZnSiO_3$ and $MnSiO_3$, at least under the experimental conditions of this work.

Zn-doped and Mn-doped enstatite were also characterized by μ -Raman spectroscopy. Both spectra of Zn and Mn-doped enstatite were compared to that one obtained from the un-doped enstatite (run H1). They showed similar behaviour, *i.e.*, a general down shifting and a broadening of the main peaks (modes at 133 and 343 cm^{-1} for Zn-doped enstatite; modes at 134, 343 and 686 cm^{-1} for Mn-doped enstatite). Both shifting and broadening increased with increasing of zinc and manganese content reflecting the modifications in local arrangements induced by the presence of impurities (*i.e.*, Zn and Mn) in the crystals structure.

CL emission spectra of no-doped enstatite (run H1) and doped with increasing amount of Mn^{2+} (run EN3, 6.30%; run EN8, 9.89%) were also studied. At room temperature, no CL emission signal was obtained from un-doped enstatite, while Mn-doped enstatite spectra were characterized by a broad red band emission located at 677 nm which intensity was directly proportional to Mn content. As confirmed by Lin *et al.*, (2006), this broad band was attributed to the transition ${}^4T_1g(G) \rightarrow {}^6A_1g(S)$ of Mn^{2+} substitutional to Mg^{2+} position in enstatite (Gaft *et al.*, 2005).

Zn-doped talc characterization

XRPD results showed that non-doped talc (JCPDS 13-0558) as single phase was obtained after 160 h of reaction, at 650 °C and 2 kbar. Willemite (Zn_2SiO_4 ; JCPDS 46-1316) and quartz (SiO_2 ; JCPDS 46-1045) were also detected together with talc when ZnO was added to the starting mixture. A decrease in temperature from 650 °C (T2e) to 500 °C (T2a) yielded the same phases (talc, willemite, and quartz); a further decrease to 300 °C caused a reduction in talc crystallinity. Indeed, the temperature of hydrothermal synthesis had a strong influence on the crystallinity of the materials. XRPD patterns of the products showed that Zn-doped talc reduced its abundance when $H_2O + CaCl_2$ was used as reactant (runs T2Ca, T3Ca). Likely, $CaCl_2$ did not favor the reaction between the starting materials that mainly formed zinc oxide and silicon dioxide in addition to talc (Table 2). Conversely, the use of HCl as reactant (run T2HCl) increased the solubility of SiO_2 , improving the reaction toward a more abundant formation of talc. Moreover, XRPD data showed that on equal experimental conditions, Zn-doped talc obtained from runs altered with 12 wt.% distilled water (T2b, T2d runs) was more abundant than

that obtained from runs with 4 wt.% distilled water (T2a, T2c runs), because a complete reaction between the starting materials was achieved. Talc morphology and content of dopant within the crystals showed strong dependence on crystallization temperature. Indeed, talc obtained at 300 °C exhibited a cabbage-like morphology (Fig. 2a), crystallized in thin wavy lamellar sheets at 500 °C, and assumed its classical hexagonal morphology when temperature was increased to 650 °C (Fig. 2b).

As regards to chemical composition, SEM-EDS semi-quantitative analyses of several talc crystals from

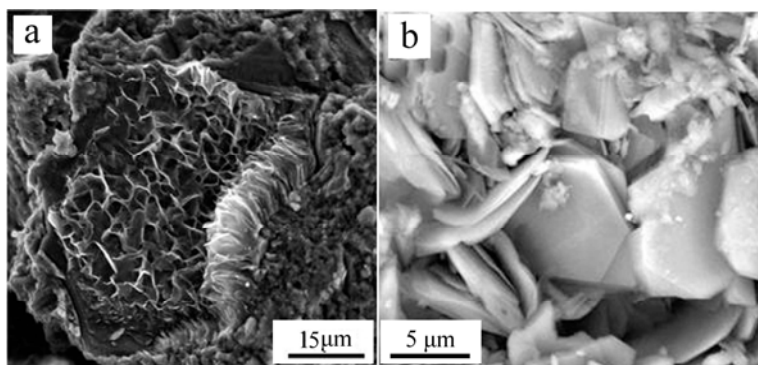


Fig. 2 - Secondary electron SEM images of two run products: (a) talc showing cabbage-like morphology; (b) talc showing classical hexagonal plate morphology.

all runs showed that the amount of Zn indicated as ZnO wt.% ranges from 5.40 to 19.35 wt.%. The content of zinc dopant increased with the decreasing of the temperature of crystallization. The Zn-doped talc was also characterized by DSC-TG and FT-IR. The lower temperature value (down to 786.1 °C; T2d run) observed for decomposition of Zn-doped sample indicated the lower thermal stability of the Zn-doped talc with respect to the pure talc which showed a breakdown at 923.6 °C (Catalano *et al.*, 2014). It is clear that the presence of zinc in talc

lattice, which has the ionic radius (0.74 Å) slightly larger than ionic radius of Mg (0.72 Å) caused defects in the Zn-doped talc that decreased its thermal stability.

The FT-IR investigation was undertaken mainly to study the detailed effects of substitutions in the octahedral layer on the hydroxyl stretching vibrations of talc. In particular, Zn-dopant in talc mainly affected the hydroxyl stretching fundamental peak (3674 cm⁻¹), splitting itself into as many as four peaks with respect to non-doped talc (Catalano *et al.*, 2014) and displaying only a sharp band in good agreement with Wilkins & Ito, (1967). The splitting appeared to be dependent on the degree of substitution of the magnesium in the octahedral layer and related to the electronegativity difference between Zn and Mg (Wilkins & Ito, 1967).

CONCLUSIONS

Enstatite single crystals doped with zinc and manganese were grown by the flux growth technique in the temperature range 600-1350 °C with lithium-vanadium-molybdate as melting agent. The slow-cooling flux has proved to be a good technique to obtain large and well-developed single enstatite crystals useful for the evaluation of the quality of the crystals obtained (*e.g.*, crystallinity, uniformity, purity). Moreover, the presence of metal ions such as zinc and manganese in the enstatite lattice make it suitable in several technological applications such as glass-ceramics (Zn-doped enstatite), red-light emitting phosphor and as microwave and millimeterwave materials (Mn-doped enstatite).

Un-doped and Zn-doped talc crystals were successfully synthesized under hydrothermal conditions. Despite the relationships between experimental conditions (temperature, pH, Zn content), lamellar size and morphology are complex, we observed that the morphology of Zn-doped talc can be controlled effectively by adjusting the experimental conditions. The possibility to control the morphology of the talc particles is a very important achievement; indeed, the morphology is one of the main physical parameters that determine whether specific talc is suitable for a specific technological application or not. This work has laid a foundation for the creation of new potentially technological materials and it opens up several avenues for future works on these materials to have a better knowledge of other physical properties for use in some specific application.

REFERENCES

- Bloise, A., Belluso, E., Fornero, E., Rinaudo, C., Barrese, E., Capella, S. (2010): Influence of synthesis conditions on growth of Ni-doped chrysotile. *Micropor. Mesopor. Mater.* **132**, 239-245.
- Bloise, A., Pingitore, V., Miriello, D., Apollaro, C., Armentano, D., Barrese, E., Oliva, A. (2011): Flux growth and characterization of Ti- and Ni-doped enstatite single crystals. *J. Cryst. Growth*, **329**, 86-91.
- Catalano, M., Belluso, E., Miriello, D., Barrese, E., Bloise, A. (2014): Synthesis of Zn-doped talc in hydrothermal atmosphere. *Cryst. Res. Technol.*, **49**, 283-289.
- Gaft, M., Reisfeld, R., Panczer, G. (2005): Modern luminescence spectroscopy of minerals and materials. Springer (Ed.), Berlin, Heidelberg, New York. 332 p.
- Höland, W & Beall, G.N. (2002): Glass-Ceramic Technology. The American Ceramic Society, Westerville, Ohio. 372 p.
- Ishida, K. (1990): Identification of infrared OH librational bands of talc-willemseite solid solution and Al (IV)-free amphiboles through deuteration. *Mineral. J.*, **15**, 93-104.
- Kirak, A., Yilmaz, H., Guler, S., Guler, C. (1999): Dielectric properties and electric conductivity of talc and doped talc. *J. Phys. D: Appl. Phys.*, **32**, 1919-1927.
- Lin, L., Min, Y., Chaoshu, S., Weiping, Z., Baogui, Y. (2006): Synthesis and Luminescence Properties of Red Phosphors: Mn²⁺ Doped MgSiO₃ and Mg₂SiO₄ Prepared by Sol-Gel Method. *J. Rare Earths*, **24**, 104-107.
- Moncorgè, R., Bettinelli, M., Guyot, Y., Cavalli, E., Capobianco, J.A., Girard, S. (1999): Luminescence of Ni²⁺ and Cr³⁺ centres in MgSiO₃ enstatite crystals. *J. Phys. Condens. Matter*, **11**, 6831-6841.
- Ohsato, H. (2004): Microwave ceramics and devices for ubiquitous computing. *Seramikkusu*, **39**, 578-583.
- Pidluzhna, A.Y., Grigorochak, I.I., Nikipanchuk, M.V., Ostafiychuk, B.K., Budzulyak, I.M., Mitsov, M.M., Yablon, L.S. (2012): Intercalation current in oxygen- and sulfur-doped talc. *Russ. J. Electrochem.*, **48**, 545-602.
- Sangwal, K. (1996): Effects of impurities on crystal growth processes. *Prog. Crystal Growth Ch.*, **32**, 3-43.
- Smyth, J.R. & Ito, J. (1977): The synthesis and crystal structure of magnesium-lithium-scandium-protophyroxene. *Am. Mineral.*, **62**, 1252-1257.
- Song, M.E., Kim, J.S., Joung, M., Nahmw, R.S., Kim, Y.S., Paik, J.H., Choi, B.H. (2008): Synthesis and Microwave Dielectric Properties of MgSiO₃ Ceramics. *J. Am. Ceram. Soc.*, **91**, 2747-2750.
- Sun, G.N. & Kim, E.S. (2012): Microwave Dielectric Properties of Diopside-Enstatite Glass-Ceramics. *Ferroelectrics*, **434**, 44-51.
- Turner, F.J., Heard, H., Griggs, D.T. (1960): Experimental deformation of enstatite and accompanying inversion to clinoenstatite. XXI International Geological Congress, Copenhagen, **18**, 399-408.
- Ushio, M., Kobayashi, N., Suzuki, M., Sumiyoshi, Y. (1991): Crystal growth of Mg₂SiO₄ and MgSiO₃ single crystals by the flux method. *J. Am. Ceram. Soc.*, **74**, 1654-1657.
- Wilkins, R.W. & Ito, T. (1967): Infrared spectra of some synthetic talcs. *J. Am. Mineral.*, **52**, 1649-1661.